Biol Cybern (2015) 109:597–610
DOI 10.1007/s00422-015-0663-5

ORIGINAL ARTICLE

Biological Cybernetics

Spatiotemporal synchronization of biped walking patterns with multiple external inputs by style–phase adaptation

Takamitsu Matsubara[1,2] · **Akimasa Uchikata**[1,2] · **Jun Morimoto**[1]

Received: 19 January 2015 / Accepted: 29 September 2015 / Published online: 12 October 2015

Abstract In this paper, we propose a framework for generating coordinated periodic movements of robotic systems with *multiple* external inputs. We developed an adaptive pattern generator model that is composed of a two-factor observation model with a *style parameter* and phase dynamics with a *phase variable*. The style parameter controls the spatial patterns of the generated trajectories, and the phase variable manages its temporal profiles. By exploiting the style–phase separation in the pattern generation, we can independently design adaptation schemes for the spatial and temporal profiles of the pattern generator to multiple external inputs. To validate the effectiveness of our proposed method, we applied it to a user–exoskeleton model to achieve user-adaptive walking assistance for which the exoskeleton robot's movements need to be coordinated with the user walking patterns and environment. As a result, the exoskeleton robot successfully performed stable biped walking behaviors for walking assistance even when the style of the observed walking pattern and the period were suddenly changed.

Keywords Style–phase adaptation · Spatiotemporal synchronization · Biped walking · Teleoperation

✉ Takamitsu Matsubara
takam-m@is.naist.jp; takam-m@atr.jp

Jun Morimoto
xmorimo@atr.jp

[1] Department of Brain Robot Interface, ATR Computational Neuroscience Laboratories, Kyoto, Japan

[2] Nara Institute of Science and Technology (NAIST), Nara, Japan

1 Introduction

Sensory–motor coordination for generating coordinated periodic movements of robotic systems with external sensory inputs is becoming crucial for applications that include interactions among humans, robots and the environment. Since wearable robots have physical contact with human users, using predefined joint angle trajectories to control the robots are not optimal. Therefore, an adaptive coordination mechanism of robot control to the external inputs is important.

Such an issue has been mainly addressed in legged locomotion with oscillator-based controllers (Taga et al. 1991; Fukuoka et al. 2003; Endo et al. 2004; Nakanishi et al. 2004; Tsuchiya et al. 2003). So that the locomotion behaviors are robust against perturbations and rough terrains, the controller is coordinated with the environmental situations through sensory signals (Taga et al. 1991; Fukuoka et al. 2003; Endo et al. 2004) or by resetting the oscillator phase when a robot foot touches the ground (Nakanishi et al. 2004; Tsuchiya et al. 2003).

Other applications, such as drumming (Kotosaka and Schaal 2000) or generating gestures for human–robot communication (Kanda et al. 2003; Michalowski et al. 2007), also use the adaptive coordination approach. In exoskeleton robot control, the robot's center of pressure (CoP) is utilized to estimate user intentions and then as a trigger in a finite-state machine controller for user-adaptive walking support (Suzuki et al. 2007). Other works (Zhang and Hashimoto 2009; Ronsse et al. 2010, 2011) utilize oscillator-based controllers with coordination to user intentions through sensory signals, as in similar works for legged locomotion control (Fukuoka et al. 2003; Endo et al. 2004; Nakanishi et al. 2004).

The oscillator-based controllers in these studies, however, suffer from their own limitations. The neural oscillator model (Matsuoka 1985) used in various researches (Fukuoka et al.

2003; Endo et al. 2004; Kotosaka and Schaal 2000; Zhang and Hashimoto 2009) requires careful parameter turning or optimization possibly by reinforcement learning methods (Matsubara et al. 2006; Endo et al. 2008; Nakamura et al. 2007) or genetic algorithms (Hase and Yamazaki 1998). The phase oscillator model (Nakanishi et al. 2004; Tsuchiya et al. 2003) only focuses on the temporal profiles of the controller. More recently, a combination of an oscillator-based CPG and dynamic movement primitives (Li et al. 2014) or combination of a set of phase-oscillator-based CPG models (Matos and Santos 2014) has been investigated. However, still, their parameter turning processes require computationally intensive nonlinear optimization methods as in André et al. (2015) and Silva et al. (2014). We were motivated by such difficulties of the previous approaches to develop a flexible and scalable method which can automatically adapt to human behaviors and environmental conditions.

As related works, adaptive frequency oscillator models (Righetti et al. 2006; Righetti and Ijspeert 2006; Gams et al. 2009) were proposed for adaptive coordination with such "high-level features" as amplitude, frequency and offset of a periodic pattern. Since these methods are designed to be used to imitate spatial and temporal motion profiles of a human demonstrator movement, they only need to take a single external input observed from the solo human demonstrator into account. On the other hand, in many situations, robot movements need to be coordinated with more than one external input. For example, a movement of a communication robot can be required to be synchronized with surrounding people than only one person, or a humanoid robot can be required to imitate a human demonstrator movement while the robot movement need to be coordinated with the external sensory inputs that represent the contact information with the surrounding environment.

In this paper, we propose an adaptive pattern generator model for generating coordinated periodic movements of robotic systems with *multiple* external inputs. The main contribution of our model is on its unique structure based on the *style–content separation* (Tenenbaum and Freeman 2000; Brand and Hertzmann 2000; Wang et al. 2007; Taylor and Hinton 2009; Matsubara et al. 2011, 2012), which allows online automatic adaptation of the parameters of the pattern generator to multiple external inputs. The key idea of our model is separating the pattern adaptation technique into spatial and temporal factors. The adaptive pattern generator model is composed of a two-factor (style and phase) observation model with *style parameter* and phase dynamics. In this paper, we define the term "style" as the spatial features of a movement, which is independent of the temporal features, and the features are mathematically defined in Eq. (2). Therefore, the definition can be different from that of other biological studies. The style parameter controls the spatial patterns of the generated trajectories, and the phase variable controls its temporal profiles. With the proposed model, the spatial and temporal patterns of the generated trajectories can be *independently* coordinated with external inputs. For coordinating such a pattern generator with human behaviors or environmental conditions, we estimate both the phase variable and the style parameter from sequential observations using a computationally efficient online expectation–maximization (EM) algorithm. An overview of our style–phase adaptive pattern generator model is depicted in Fig. 1.

Recently, the separation of the CPG adaptation into temporal and spatial profiles has been addressed in humanoid robot locomotion (Degallier et al. 2011; Nassour et al. 2014), in which the spatial and temporal features of the generated patterns can be independently and manually modified by using different parameters. However, to generate walking patterns for an exoskeleton, an automatic parameter adaptation scheme to observed human walking movements is required. This kind of parameter learning procedure has not been addressed in the previous studies possibly due to the complex structure of the CPG model. On the other hand, in our proposed method, the style and phase parameters can be automatically adapted to the observed movements.

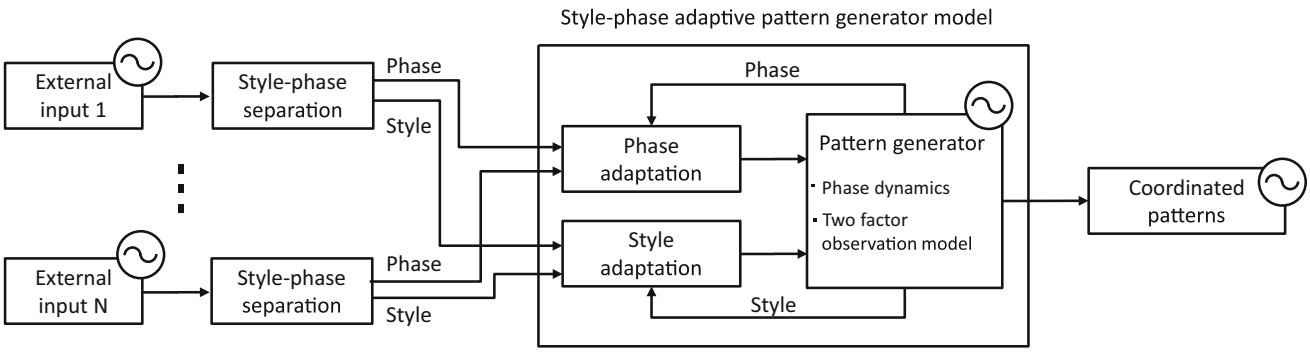

Fig. 1 Overview of style–phase adaptive pattern generator model for spatiotemporal synchronization of periodic patterns with *multiple* external inputs. Pattern generator model is composed of a two-factor observation model with style parameter and phase dynamics with phase variable. By taking advantage of the style–phase separation in pattern generation, we can independently design adaptation schemes for spatial and temporal profiles of a pattern generator to multiple external inputs

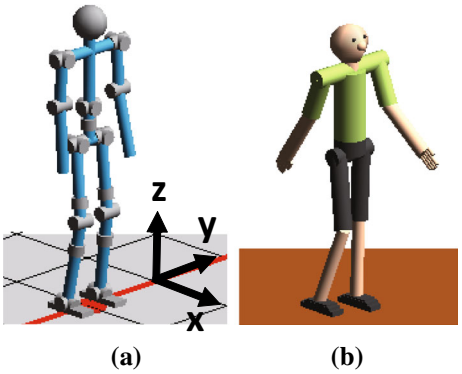

Fig. 2 Humanoid robot and human models. **a** Humanoid model with a 22-DOF floating-base rigid body dynamics. Physical interactions between robot feet and ground are also included in simulation. **b** Human model with a fixed-base on the torso. Both robots are 1.58 m high and weigh 60 kg

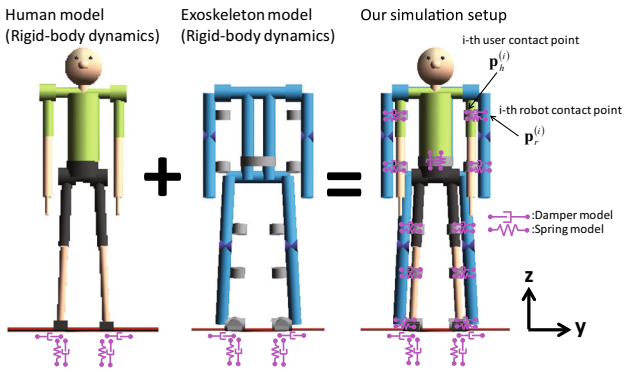

Fig. 3 User–exoskeleton model. User and full-body exoskeleton robot are both modeled by a 1.58-m-high, 60 kg model with a 22-DOF floating-base rigid body dynamics. Physical interactions among user model, robot model and environment are introduced by simulating three kinds of forces applied to user and robot as joint torque, ground reaction force and constraint force caused by physical coupling between user and robot at each contact point

We first show how our proposed adaptive pattern generator model works using human and humanoid models (Fig. 2). Using these two simulated models, we show that the humanoid model can adaptively imitate the movements of the human model, and the ground contact, which represents interaction between the humanoid and the environment, is explicitly considered. Successful results of imitation tasks with using our proposed adaptive pattern generator encouraged us to apply our proposed method to predict human user movements to assist user behaviors. Thus, we developed a user–exoskeleton model (Fig. 3), where the human user and the exoskeleton robot models are physically connected using three-dimensional forces simulated by a three-dimensional spring–damper model as physical coupling forces at each contact point per link to connect between the user and the robot. Its details are shown in Sect. 4.1.

The paper is organized as follows. Section 2 introduces the style–phase adaptive pattern generator model for spatial and temporal coordination to the external inputs. Section 3 explains how we apply our proposed style–phase adaptive pattern generation method to design the walking controllers of humanoid and exoskeleton robots that can be coordinated with environmental dynamics and human movements. Section 4 presents the simulation setups and results with two simulation platforms. In the walking assistance simulation, the necessary torque for the user walking movements was reduced around 40 % with our proposed method.

2 Adaptive pattern generator with style–phase adaptation

2.1 Adaptive pattern generator model

We present our adaptive pattern generator model in this section. More concretely, we present a learning procedure of the model from a variety of successful motion trajectories as a data set and phase and style adaptation schemes.

2.1.1 The model

We first present the adaptive pattern generator model:

$$\dot{\phi}_c = \omega_c, \tag{1}$$

$$\mathbf{y}_c = g(\phi_c, \mathbf{w}_c) = \sum_{j=1}^{J} w_{c,j}\mathbf{f}_j(\phi_c) \tag{2}$$

where Eq. (1) is the phase dynamics and Eq. (2) is the two-factor observation model that maps phase variable ϕ_c to the joint angle vector of a robot $\mathbf{y}_c \in \mathbb{R}^D$ as the output of the pattern generator model.

The functions $\{\mathbf{f}_j(\phi_c)\}_{j=1}^{J}$ of phase variable ϕ_c in Eq. (2) are referred as the *observation bases* that span the subspace of spatial variations of the output. The parameter vector $\mathbf{w}_c = \left(w_{c,1}, \ldots, w_{c,J}\right)^\top \in \mathbb{R}^J$, often referred as *style*, is a linear coefficient vector of the observation bases. Thus, we call this as the style parameter. Various motions with different spatial features, such as large swinging of arms or much bending the elbow joints, can be generated by specifying the style parameters $\mathbf{w}_c$.

2.1.2 Learning observation model

To learn the observation model in Eq. (2), we collect multiple motion sequences $\mathcal{D} = \left\{\mathbf{Y}^1, \ldots, \mathbf{Y}^S\right\}$ that contain a diversity of motion styles. Let $\mathbf{Y}^s = [\mathbf{y}_1^s \cdots \mathbf{y}_{L_s}^s]^T \in \mathbb{R}^{L_s \times D}$ denote a motion sequence with a distinct style, where $s \in \{1, 2, \ldots, S\}$ is the style index, $c \in \{1, 2, \ldots, L_s\}$ is the

content index that corresponds to the phase, L_s is the number of data samples in the sth motion sequence, and $\mathbf{y}_c^s \in \mathbb{R}^D$ is an observation with the style indexed by s and content c.

The learning procedure is composed of the following three steps:

i) Data alignment by phase information.
ii) Extraction of observation bases.
iii) Learning a two-factor observation model.

The detailed algorithms are provided in "Appendix 1."

2.2 Phase adaptation scheme for temporal coordination

Here we present the phase adaptation scheme to adapt the phase variable of the adaptive pattern generator model to that of external inputs.

We consider the behavior of three-dimensional coupled-phase oscillator of $\{\phi_1, \phi_2, \phi_3\}$. To this end, we introduce a *step-by-step approach* for designing mutual coupling in the system. We first consider only two-dimensional phase $\{\phi_1, \phi_2\}$ out of three-dimensional coupled system $\{\phi_1, \phi_2, \phi_3\}$ using the analytical result (as summarized in "Appendix 2"). If the two oscillator system is properly coupled (i.e., it satisfies $|\omega_1 - \omega_2| < K_1 + K_2$), it behaves as just one combined system with the phase difference $\Phi^* = |\phi_2 - \phi_1|$ and the compromise frequency ω^*. Based on this, we consider one additional oscillator ϕ_3 to the coupled system of $\{\phi_1, \phi_2\}$ as:

$$\dot{\phi}_1 = \omega^* + K_3 \sin(\phi_3 - \phi_1), \tag{3}$$

$$\dot{\phi}_2 = \omega^* + K_3 \sin(\phi_3 - \phi_1), \tag{4}$$

$$\dot{\phi}_3 = \omega_3 + K_4 \sin(\phi_1 - \phi_3). \tag{5}$$

Since this three-dimensional coupled system can be interpreted as the two coupled system of ϕ_3 and $\{\phi_1, \phi_2\}$, we can approximately analyze its behavior as if $|\omega^* - \omega_3| < K_3 + K_4$, the coupled oscillator runs with the phase difference $\phi^{**} = \phi_1 - \phi_3 = \phi_2 - \Phi^* - \phi_3$ and with its compromise frequency $\omega^{**} = (K_3\omega_3 - K_4\omega^*)/(K_3 + K_4)$.

The simple simulation of the above three-dimensional case is shown in Fig. 4. The phase differences and the frequency of the coupled system are converged to the derived results of Φ^*, Φ^{**} and ω^{**}.

Based on the coupled-phase oscillator models, we propose a phase adaptation scheme of the adaptive pattern generator model for the phase variables of external inputs as follows:

$$\dot{\phi}_c = \omega_c + \sum_{i=1}^{N} K_i \sin(\phi_i - \phi_c) \tag{6}$$

where ϕ_i is the phase variable of ith system and N is the number of external inputs.

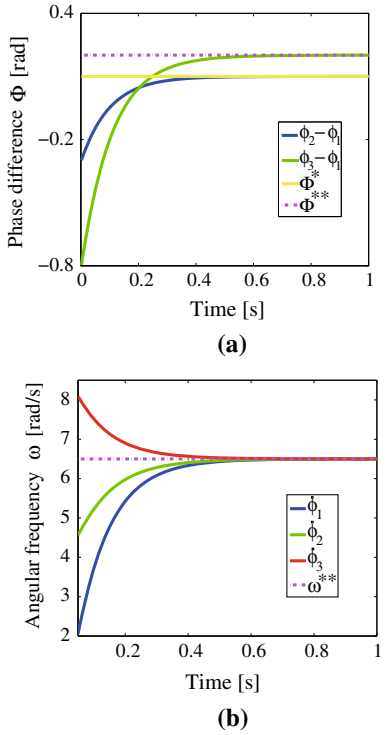

Fig. 4 Behaviors of the three-dimensional coupled-phase oscillator

2.3 Style adaptation scheme for spatial coordination

For spatial coordination of pattern generator to the external inputs, we propose a simple adaptation law for the style variable as follows:

$$\dot{\mathbf{w}}_c = \sum_{i=1}^{N} \mathbf{K}_{w,i}(\mathbf{w}_i - \mathbf{w}_c) \tag{7}$$

where $\mathbf{w}_c$ is the style parameter of the observation model in Eq. (2), $\mathbf{w}_i$ is the style parameter of the ith external input, and N is the number of external inputs. The gain matrix $\mathbf{K}_{w,i} = k_{w,i}\mathbf{I}$ is set as a diagonal matrix. The parameter $k_{w,i}$ controls the trade-off between the convergence speed of the adaptation and the stability of the system; a larger value accomplishes higher convergence speed, while it may result in unstable behaviors and vice versa. Therefore, we empirically set it as much as possible to increase with certain stability.

3 Coordinated walking pattern generation for humanoid and exoskeleton robots

From this section, we focus on the application of our proposed method to the humanoid and exoskeleton robot models for generating biped walking behaviors coordinated with multiple external inputs.

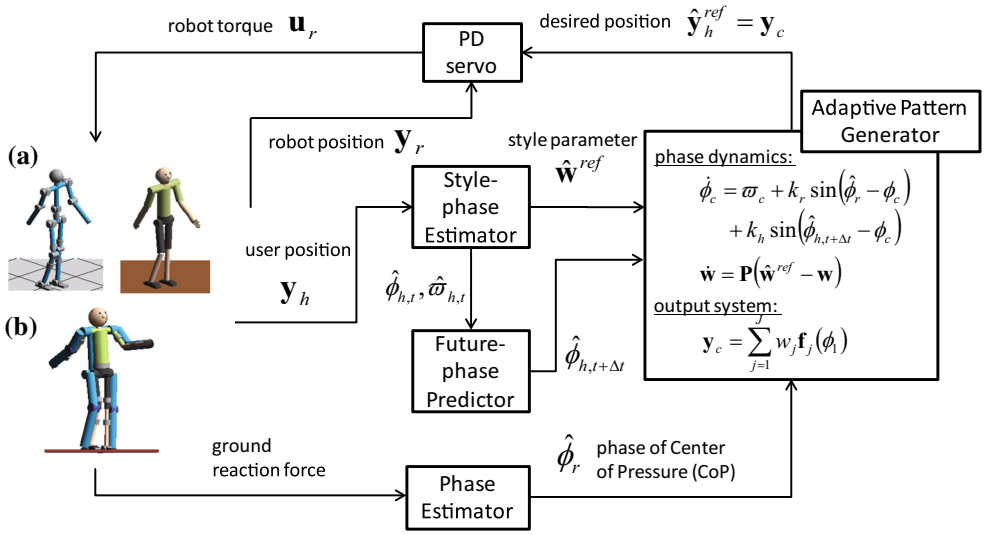

Fig. 5 Schematic diagram of our adaptive walking assistance strategy to control a full-body humanoid robot and an exoskeleton robot. Control scheme is mainly comprised of four components: (1) adaptive pattern generator, (2) style–phase estimator for user motions, (3) its future-phase predictor, and (4) phase estimator of a CoP trajectory. The adaptive pattern generator is spatiotemporally coordinated with user motions and Center of Pressure (CoP) trajectories of the robot feet to generate trajectories as references to the robot controller, which outputs joint torques to the user as assistance

3.1 Walking controller with adaptive pattern generator

The schematic diagram of the constructed walking controller is depicted in Fig. 5. In this case, a human walking pattern corresponds to a set of joint angle trajectories of the human, and the environmental information means the ground reaction force applied to the robot, which is detected as sensory signals. We estimate the style and phase variables from the observed human walking patterns and the phase variable from the ground reaction force to coordinate the robot movements by the adaptive pattern generator with style–phase adaptation schemes in Eqs. (6) and (7).

Our method assumes the same kinematic structure between the human model and the robot model regarding the number of DOFs and length of each link. We can possibly overcome such a limitation by properly modeling the difference between them: one possible approach is to construct a bidirectional mapping between the human's and the robot's poses through a shared low-dimensional space to be used for style–phase adaptation (Michalowski et al. 2012).

3.2 Style–phase estimation for user motions

The state variable is composed of the phase ϕ_h and its velocity ω_h of user motion as $\mathbf{x} = [\phi_h \ \omega_h]^T$, and the following algorithm estimates a time series of state variable $\hat{\mathbf{X}} = [\hat{\mathbf{x}}_1 \cdots \hat{\mathbf{x}}_T]^T$ and style parameter vector $\hat{\mathbf{W}}_h = [\hat{\mathbf{w}}_{h,1} \cdots \hat{\mathbf{w}}_{h,T}]^T$ from a portion of user motion $\hat{\mathbf{Y}}_h = [\hat{\mathbf{y}}_{h,1} \cdots \hat{\mathbf{y}}_{h,T}]^T$ in an online manner.

3.2.1 Generative model

Here we define a generative model of user motion using the two-factor observation model defined in Eq. (2). By assuming additive Gaussian noise in the phase transition and the observation, we set the generative model of motion as

$$p(\mathbf{x}_{t+1}|\mathbf{x}_t) = \mathcal{N}(\mu_x(\mathbf{x}_t), \mathbf{Q}), \tag{8}$$

$$p(\mathbf{y}_{h,t}|\mathbf{z}_t; \mathbf{w}_h) = \mathcal{N}(\mu_y(\mathbf{z}_t; \mathbf{w}_h), \mathbf{R}) \tag{9}$$

where $\mu_y(\cdot; \mathbf{w}_h) = g(\cdot, \mathbf{w}_h)$ in Eq. (2), $\mu_x(\mathbf{x}) = \mathbf{A}\mathbf{x}$ and the state transition matrix is $\mathbf{A} = \begin{bmatrix} 1 & 1 \\ 0 & 1 \end{bmatrix}$, $\mathbf{Q}$ and $\mathbf{R}$ are the covariance of the additive Gaussian noise in the state transition and the observation, respectively.

3.2.2 Online estimation of state variable and style parameter

The derived online update laws of the estimation of the state and style variables can be summarized as (Matsubara et al. 2012):

$$\hat{\mathbf{x}}_t \leftarrow U(\hat{\mathbf{x}}_{t-1}, \hat{\mathbf{w}}_{h,t}, \hat{\mathbf{y}}_{h,t}), \tag{10}$$

$$\hat{\mathbf{w}}_{h,t} \leftarrow V(\hat{\mathbf{w}}_{h,t-1}, \hat{\mathbf{x}}_t, \hat{\mathbf{y}}_{h,t}; \lambda) \tag{11}$$

where parameter $\lambda(t)(0 \leq \lambda(t) \leq 1)$ is a time discounting factor that is introduced to forget the effect of the old posterior values. If we set $\lambda(t) = \lambda < 1.0$, this can be applied for

non-stationary motion sequences. The details of the update rules (i.e., E-step: $U(\cdot)$ and M-step: $V(\cdot)$) are explained in "Appendix 3."

3.2.3 Phase predictor

The future phase of user motions can be easily predicted by using the estimated phase and its velocity as:

$$\hat{\phi}_{h,t+\triangle t} = \hat{\phi}_{h,t} + \hat{\omega}_{h,t}\triangle t \tag{12}$$

where $\triangle t$ is the prediction step size.

For the online adaptation of style and phase variables, we use the first-order phase dynamics model in our framework. Therefore, the prediction is performed for only one step because one-step prediction and multi-step predictions with a smaller step size give us the same results due to the linearity of the first-order model. Selection of the prediction step size can affect the performance of walking assistance. Therefore, we empirically investigated its effect as presented in Sect. 4.4.

The predicted movements of a recognized user motion can be used to compensate feedback delay for generating assistive movements for user motions.

3.3 Phase estimator for environment

Since the walking behavior is periodic, a periodic pattern of the CoP of the feet is observed and can be used to estimate the phase of the environment $\hat{\phi}_r$ (Morimoto et al. 2008):

$$\hat{\phi}_r = -\arctan\left(\frac{\dot{p}}{p}\right) \tag{13}$$

where p denotes the CoP.

By using the force sensors on the feet, the CoP can be detected as

$$p = \frac{p^{\mathrm{l}}_{\mathrm{foot}} F^{\mathrm{l}}_z + p^{\mathrm{r}}_{\mathrm{foot}} F^{\mathrm{r}}_z}{F^{\mathrm{r}}_z + F^{\mathrm{l}}_z} \tag{14}$$

where F^{l}_z and F^{r}_z represent the left and right ground reaction force, and $p^{\mathrm{l}}_{\mathrm{foot}}$ and $p^{\mathrm{r}}_{\mathrm{foot}}$ are the lateral position of each foot, respectively. Its derivative $\dot{p}$ is calculated by numerical differentiation as $\dot{p} \approx \frac{p_{t+1}-p_t}{\triangle t}$ where $\triangle t$ is the discrete time step. The notations are illustrated in Fig. 6.

4 Simulation and results

This section shows our simulation setup and results for evaluating our robot control scheme. As explained in Sect. 1, we apply our scheme for two physical simulation platforms:

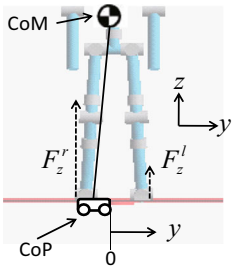

Fig. 6 Inverted pendulum dynamics model

(1) the humanoid and human models and (2) the physically coupled user–exoskeleton robot model, as depicted in Figs. 2 and 3, respectively.

4.1 Simulation setup

We simulate the human user, the humanoid robot and the full-body exoskeleton robot behaviors by using a 22-DOF floating-base rigid body dynamics. Furthermore, we introduce physical interactions between the user model and the robot model.

We use a PD controller to calculate the joint torques to track the reference as follows:

$$\mathbf{u}_h = \mathbf{K}_p(\mathbf{y}^{\mathrm{ref}}_h - \mathbf{y}_h) - \mathbf{K}_d\dot{\mathbf{y}}_h, \tag{15}$$

where $\mathbf{y}^{\mathrm{ref}}_h \in \mathbb{R}^D$ is the user reference position of all the joints and $\mathbf{K}_p$, $\mathbf{K}_d$ are gain matrices.

The ground reaction forces to the feet are separately modeled in the vertical and horizontal directions. The vertical ground reaction force at a contact point is simulated by a spring–damper model given by

$$f^{(k)}_z = -k^z_p z^{(k)}_{\mathrm{cp}} - k^z_d \dot{z}^{(k)}_{\mathrm{cp}}, \tag{16}$$

where k^z_p is the spring gain, k^z_d is the damper gain, $z^{(k)}_{\mathrm{cp}}$ denotes the vertical position of a contact point on the feet, and $k \in \{1, \ldots, K\}$ indicates the index of the contact points. We set $K = 8$ for all the corners of both feet.

The horizontal reaction forces on a contact point are simulated by viscous friction models as

$$f^{(k)}_x = -k^x_d \dot{x}^{(k)}_{\mathrm{cp}} \tag{17}$$

$$f^{(k)}_y = -k^y_d \dot{y}^{(k)}_{\mathrm{cp}}, \tag{18}$$

where k^x_d, k^y_d are damper gains and $x^{(k)}_{\mathrm{cp}}$, $y^{(k)}_{\mathrm{cp}}$ are the horizontal positions of the kth contact point on the feet. These ground reaction forces are applied when $z^{(k)}_{\mathrm{cp}} < 0.0$ is satisfied. When the user wears the exoskeleton robot, several parts of the user's body need to be physically coupled to the corresponding parts of the robot to receive the effect of motion assistance. The constraint force caused by the physical coupling between a set of constraint points of the user and the

robot is simulated by a spring–damper model as

$$\mathbf{f}_{\mathrm{cs}}^{(i)} = \mathbf{K}_p^{\mathrm{cs}}(\mathbf{p}_r^{(i)} - \mathbf{p}_h^{(i)}) - \mathbf{K}_d^{\mathrm{cs}}\dot{\mathbf{p}}_h^{(i)}, \tag{19}$$

where $\mathbf{f}_{\mathrm{cs}}^{(i)} \in \mathbb{R}^3$ is the constraint force applied at $\mathbf{p}_h^{(i)} \in \mathbb{R}^3$ of the user from $\mathbf{p}_r^{(i)} \in \mathbb{R}^3$ of the robot. $i \in \{1, \ldots, I\}$ indicates the index number of a set of constraint points. As shown in Fig. 3, we set $I = 11$ for our setup. $\mathbf{K}_p^{\mathrm{cs}}$ and $\mathbf{K}_d^{\mathrm{cs}}$ are the spring and damper gains. The model coefficients can be interpreted as how tight/loose the physical couplings are.

4.2 Generation of simulated human walking patterns

We use simulated human walking patterns generated by using the robot simulators so that we can precisely evaluate generated joint torques by the human user model. To this end, we implemented a sinusoidal pattern-based biped walking controller on the simulated robot proposed by Morimoto et al. (2008) with 2 kHz control period. Then, by changing a number of free parameters such as the amplitudes of the periodic patterns and the bias terms for selected joints, in total, we produced 26 different walking sequences with different motion styles as the data set $\mathcal{D}$ introduced in Sect. 2.1.2. Using this data set, we applied the learning procedure presented in Sect. 2.1 and obtained the adaptive pattern generator model of the robot with six-dimensional style parameter as $J = 6$ that was determined so that it represents more than 98 % of the produced training data.

4.3 Spatiotemporal coordination of humanoid walking with user motions and environment

We prepared three different simulated human walking patterns by using the dynamical simulator and use these synthesized walking patterns as the observation sequence from the user model as the test data for evaluation. The first motion is switched to the second at 25 s. The second motion is switched to the third at 37.5 s (See Fig. 7a). The covariance matrices in the generative model for estimating observed motion phase and style were set as $\mathbf{Q} = \mathrm{diag}\{0.001, 0.01\}$, $\mathbf{R} = 0.2\mathbf{I}$.

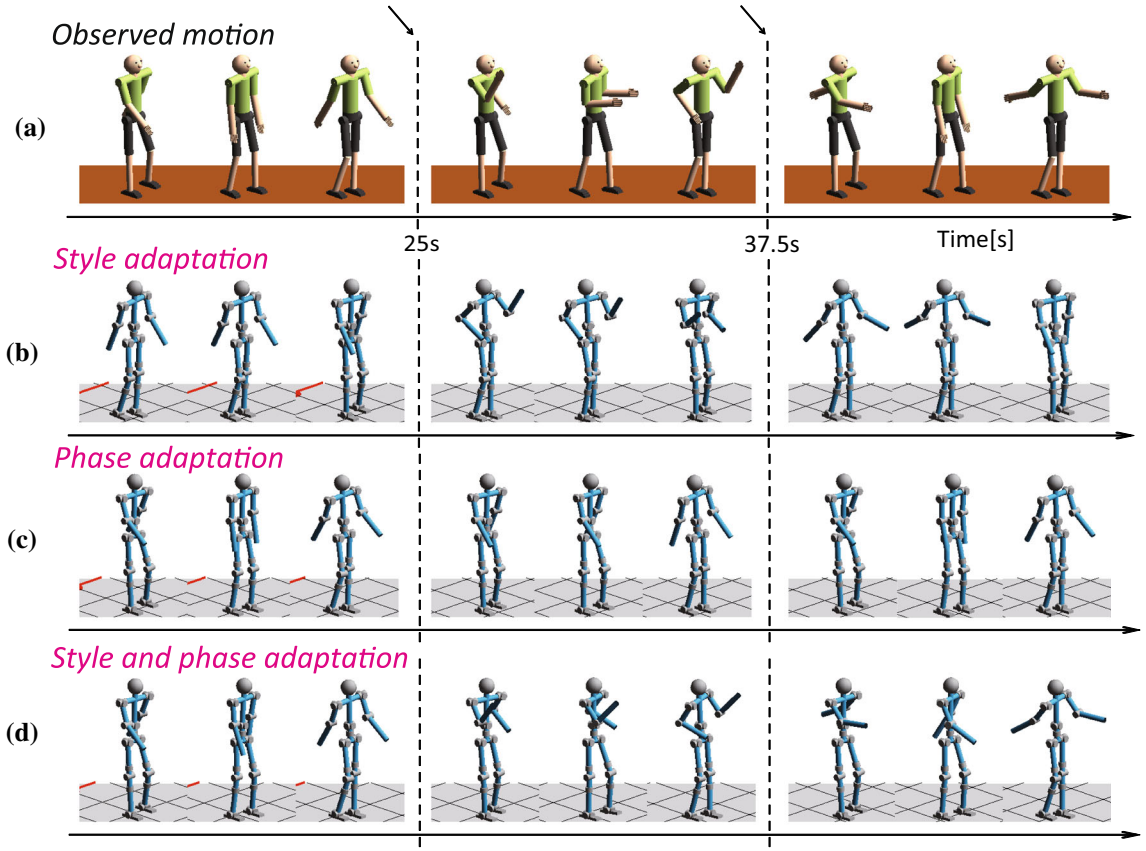

Fig. 7 Successful walking behaviors of the robot using our proposed method. **a** The three different observed motions. The first motion is switched to the second at 25 s. The second motion is switched to the third at 37.5 s. **b** The walking behaviors of the robot using the style adaptation with the observed motion, **c** the result using the phase adaptation with the observed motion and **d** the result using both the style and phase adaptations with observed motion. Note that in **b**–**d** the phase adaptation with the environment is also applied to keep the balance of the robot during walking behaviors

The PD servo was used to calculate the joint torques as $\mathbf{u} = \mathbf{K}_p(\mathbf{y} - \mathbf{q}) - \mathbf{K}_d\dot{\mathbf{q}}$ where $\mathbf{q}$ and $\dot{\mathbf{q}}$ are the current joint angle vector and its velocity of the robot, and each gain matrix were set as $\mathbf{K}_p = 2000\mathbf{I}$ and $\mathbf{K}_d = 100\mathbf{I}$, respectively. The forgetting factor in the EM algorithm was set as $\lambda = 0.7$.

We show the results of our proposed method for the platform as shown in Fig. 2. The snapshots of the successful walking behaviors of the robot with three different coupling parameter settings of the coordination strategies are shown in Fig. 7. The result with the parameters $\{k_h = 0, k_r = 40, k_w = 100\}$ is shown in Fig. 7b. Since the style parameter is only adapted with the observed motion, the temporal profile of the robot movement is not coordinated with observed motion. Figure 7c shows the result with the parameters $\{k_h = 30, k_r = 40, k_w = 0\}$ in which the phase variable is only adapted with the observed motion, and its spatial profile is not coordinated. Figure 7d presents the result with $\{k_h = 30, k_r = 40, k_w = 100\}$, which demonstrates that both the spatial and temporal profiles are successfully coordinated with the observed motion. For all the cases of Fig. 7b–d, the phase adaptation with the environment is applied simultaneously. Without this adaptation with the environment (e.g., $k_r = 0$), the robot could not keep stable walking and fell over as shown in Fig. 8. These results demonstrate that the spatial and temporal synchronizations of robot movements with observed motion and the environment can be independently performed using our proposed method.

The coordinated phase trajectories of the adaptive pattern generator, observed motion and the environment (in the case of Fig. 7d) is depicted in Fig. 9. Also, the estimated and adapted style parameters of the adaptive pattern generator are depicted in Fig. 10.

Figure 11 shows the averaged joint angle errors between the robot and the observed walking patterns obtained by applying the proposed method with the cases of different gain parameters as $k_h = \{10, 12.5, 30, 100\}$. We defined the error between the robot and the observed walking patterns as $E(t) = \frac{1}{D}||\mathbf{y}(t) - \mathbf{y}^h(t)||$ where D is the number of joints. The graph indicates that the error is kept as small when we set the high coupling constant in k_h because the temporal profile of the robot movement is coordinated. This suggests that we can control the effect of the adaptation by changing the values of the coupling. We observed that the robot fell over when we use too large coupling such as the coupling constant larger than $k_h = 250$.

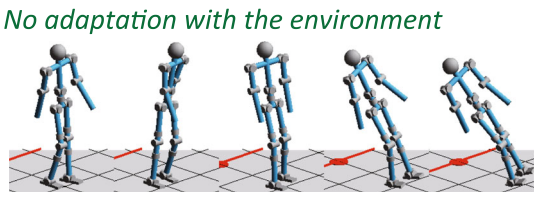

Fig. 8 Snapshots in falling over of the robot. The robot cannot walk successfully without the phase adaptation with the environment

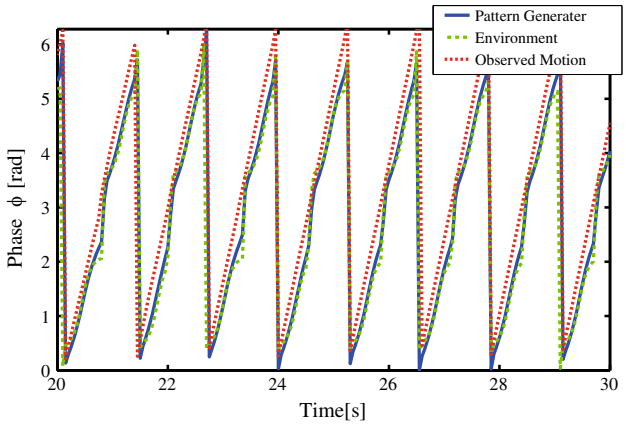

Fig. 9 Coordinated phase trajectories of the adaptive pattern generator, observed motion and the environment. Three oscillators are properly phase locked

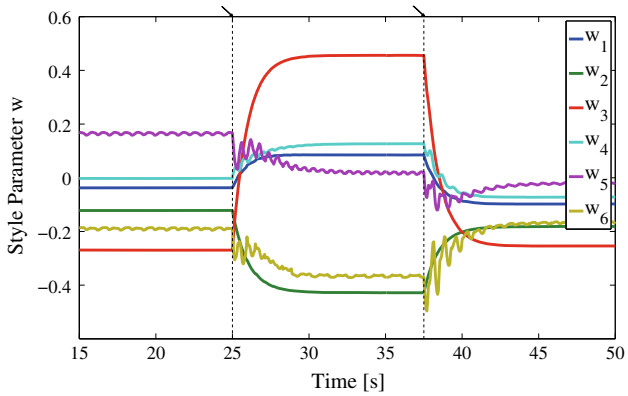

Fig. 10 Trajectories of the adapted style parameters of the adaptive pattern generators coordinated with the observed motion

4.4 Exoskeleton robot control for walking assistance

We prepared three different simulated user walking patterns (normal, running and striding) and merged them into a single non-stationary periodic movement sequence. The first motion pattern was smoothly switched to the second one at 20 s, and the second motion pattern was switched to the third one at 40 s. By setting different velocities in ω_h as 3.9, 4.2 and 4.6 rad/s, we generated three different non-stationary user walking patterns as test data to validate our method.

To investigate the effectiveness of our method, we prepared two sets of gain parameters for the human user model: (1) "high" servo gains $\mathbf{K}_p = 2000\mathbf{I}$, $\mathbf{K}_d = 10\mathbf{I}$ for the PD controller in Eq. (15) to simulate a healthy user who has sufficiently stiff joints that can track the user-intended joint trajectories, and (2) "low" servo gains $\mathbf{K}_p = 800\mathbf{I}$, $\mathbf{K}_d = 5\mathbf{I}$ to simulate a user has weakened muscles that cannot precisely

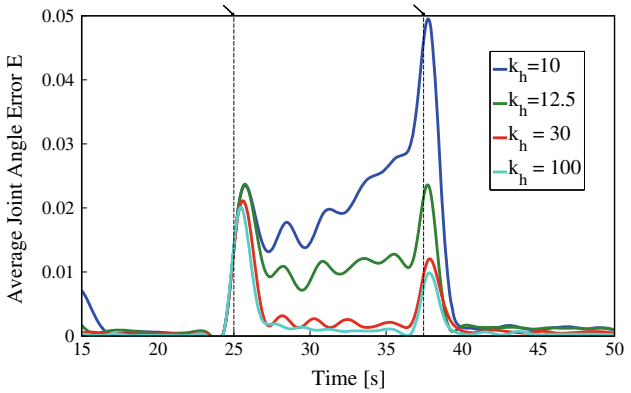

Fig. 11 Averaged joint angle errors between the robot and observed motion obtained by applying our proposed method with different values of the coupling constant k_h. Large errors are generated from 25 to 37.5 s. During this period, observed walking frequency is much faster than the frequency which can be generated by the humanoid robot model

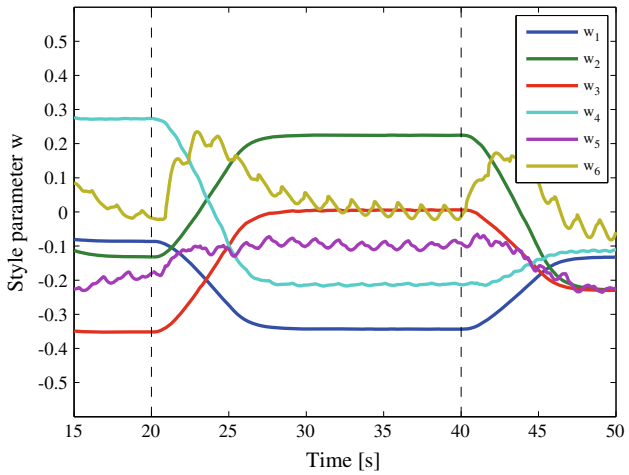

Fig. 13 Trajectories of style parameters of adaptive pattern generator during walking assistance by our control scheme. When user motion is changed at 20 and 40 s, style parameters are adapted online

track the user-intended joint trajectories. The gains for the robot motor servo were fixed as $\mathbf{K}_p = 3000\mathbf{I}$, $\mathbf{K}_d = 100\mathbf{I}$. Other gain parameters in the physical interaction models were set as $\mathbf{K}_p^{cs} = 150\mathbf{I}$, $\mathbf{K}_d^{cs} = 5\mathbf{I}$ ($\mathbf{K}_p^{cs} = 3000\mathbf{I}$, $\mathbf{K}_d^{cs} = 100\mathbf{I}$ for the feet), $k_p^z = 30000$, $k_d^x = k_d^y = 2500$, $k_d^z = 1000$. We set the following parameters in our control scheme. The covariance matrices in the generative model for estimating the observed motion phase and the style were set as $\mathbf{Q} = \mathrm{diag}\{0.001, 0.01\}$, $\mathbf{R} = 0.2\mathbf{I}$. The forgetting factor in the online state-style estimation algorithm for user motions was set as $\lambda = 0.9$. The coupling coefficients of the style and phase coordination strategies were set as $k_h = 20$, $k_r = 40$, $\mathbf{K}_w = 0.5\mathbf{I}$.

We show the results of our method applied for the platform as shown in Fig. 3. The snapshots of the successful walking behavior of the user model with a non-stationary walking pattern ($\omega_h = 4.2$) as a reference are depicted in Fig. 12a, where we set the prediction time as $\triangle t = 100$ ms. The time series of the style parameters and the phase variables are depicted in Figs. 13 and 14. These graphs show that while the user walking pattern was changed, our control scheme successfully adapted it. If one or both of these adaptations were not applied, such successful walking behaviors could not be achieved. Figure 12b, c show the results without adaptation to the CoP phase variable and to the user walking style, and for both cases, successful walking behaviors were not able to be accomplished.

Next, we show the effectiveness of our proposed method for walking assistance. Snapshots of walking behaviors with

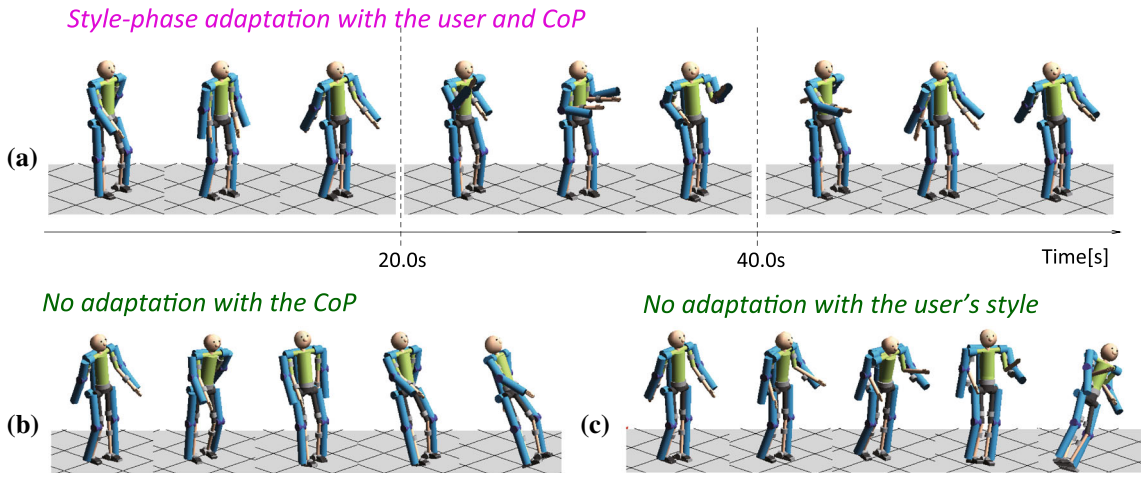

Fig. 12 Snapshots of walking behaviors of user and robot. **a** Typical example of successful walking behavior. While user walking style is changed, our control scheme successfully adapts to the new style online by style adaptation strategy in the oscillator model. **b** User and robot fall over due to no adaptation with the CoP, and **c** due to no adaptation with the user walking style

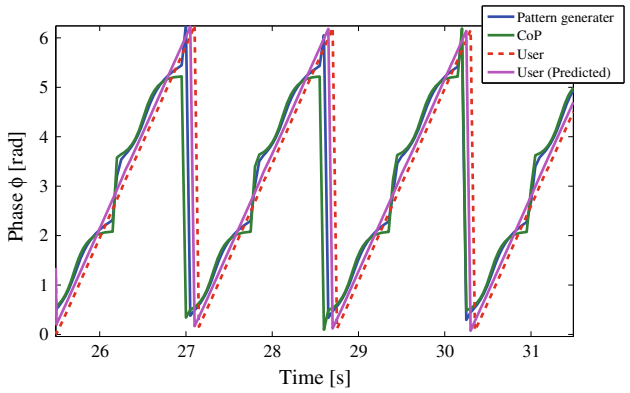

Fig. 14 Resulted trajectories of phase variables of adaptive pattern generator, CoP, user motion (current and predicted) by our control scheme. All phase variables are successfully synchronized

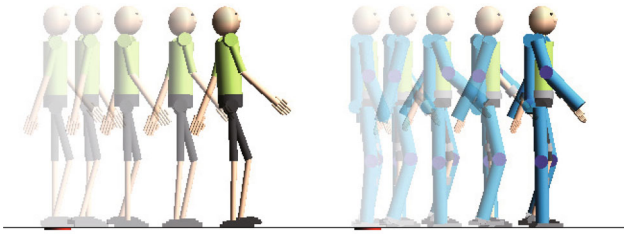

(a) High servo gains **(c)** High servo gains + assistance

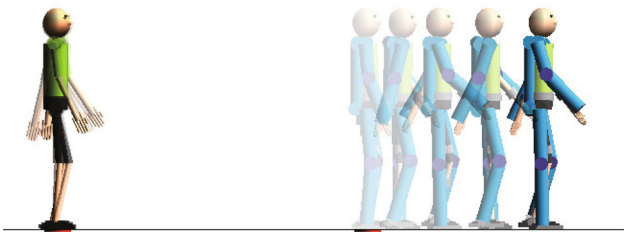

(b) Low servo gains **(d)** Low servo gains + assistance

Fig. 15 Snapshots of user walking behaviors with/without walking assistance by exoskeleton robot control. Even if user employs the low servo gains that cannot generate sufficient torques to achieve proper walking behavior as in **b**, the exoskeleton robot with our control scheme enables the user to walk as in **d**. **a** High servo gains. **b** Low servo gains. **c** High servo gains + assistance. **d** Low servo gains + assistance

and without the exoskeleton for one of the test walking patterns (normal, $\omega_h = 4.6$) are depicted in Fig. 15. Without the exoskeleton robot, coordination with the CoP trajectory is implemented for the user model to stabilize walking. Even if the user model employs the low servo gains that cannot generate sufficient torques to achieve proper walking behavior as in Fig. 12b, the exoskeleton robot with our control scheme enables the user to walk as in Fig. 12d. The representative joint trajectories with references are plotted for all the cases in Fig. 16. Here with the low servo gains, large observed tracking errors are observed due to the insufficiency of the torques in Fig. 16a. Our control scheme successfully provides assistance force to improve the tracking performance as presented in Fig. 16c.

Moreover, we investigated how the prediction time $\triangle t$ of the user motion's phase affects the performance of the walking assistance. Figure 17 shows the ratios of the averaged total torque (sum of all the joint torques) required by the user model with our control scheme to the value obtained in autonomous walking that employed the high servo gains, all of which are plotted for several cases of walking patterns, velocities and motor servo gains of the user. The graphs in the figure show that our method is useful for walking assistance, and it is more effective for the low-gain than the high-gain user model. Moreover, the prediction becomes more important when the user walking speed increases. At maximum (with the low-gain user model, 50 ms prediction time), our method reduced by around 40 % the torques required by users to walk.

As the summary, these simulation results suggest that our proposed method is useful to predict human user movements for assisting the user behaviors with an exoskeleton robot.

5 Conclusion

In this paper, we proposed a framework for generating coordinated periodic movements of robotic systems with multiple external inputs, which alleviates the limitation of the existing methods. The key idea of our approach is separating the pattern adaptation technique into the spatial and temporal factors. We proposed an adaptive pattern generator model, which is composed of the two-factor observation model with the style parameter and the phase dynamics with the phase variable. The style parameter controls the spatial patterns of the generated trajectories, and the phase variable manages its temporal profiles. By using the model, we constructed an adaptive walking assistance strategy. Our method can manage both the diversity of user motions and the interactions among the user, the robot and the environment by the style–phase adaptation scheme.

To validate the effectiveness of our proposed method, we applied it to the simulated humanoid model to perform biped walking behaviors flexibly coordinated with the observed walking patterns while the interaction with the environment was explicitly taken into account. We also applied our proposed method to the simulated exoskeleton robot model to perform stable and effective waking assistance to the user model. Simulation results validated the effectiveness of our method. The proposed method may also be applicable for patients with walking problems if we have a data set of walking patterns for various attributes of gender, body shape and condition. Our method could also be easily extended to a *multi-user interface* (Matsubara and Morimoto 2013) if we

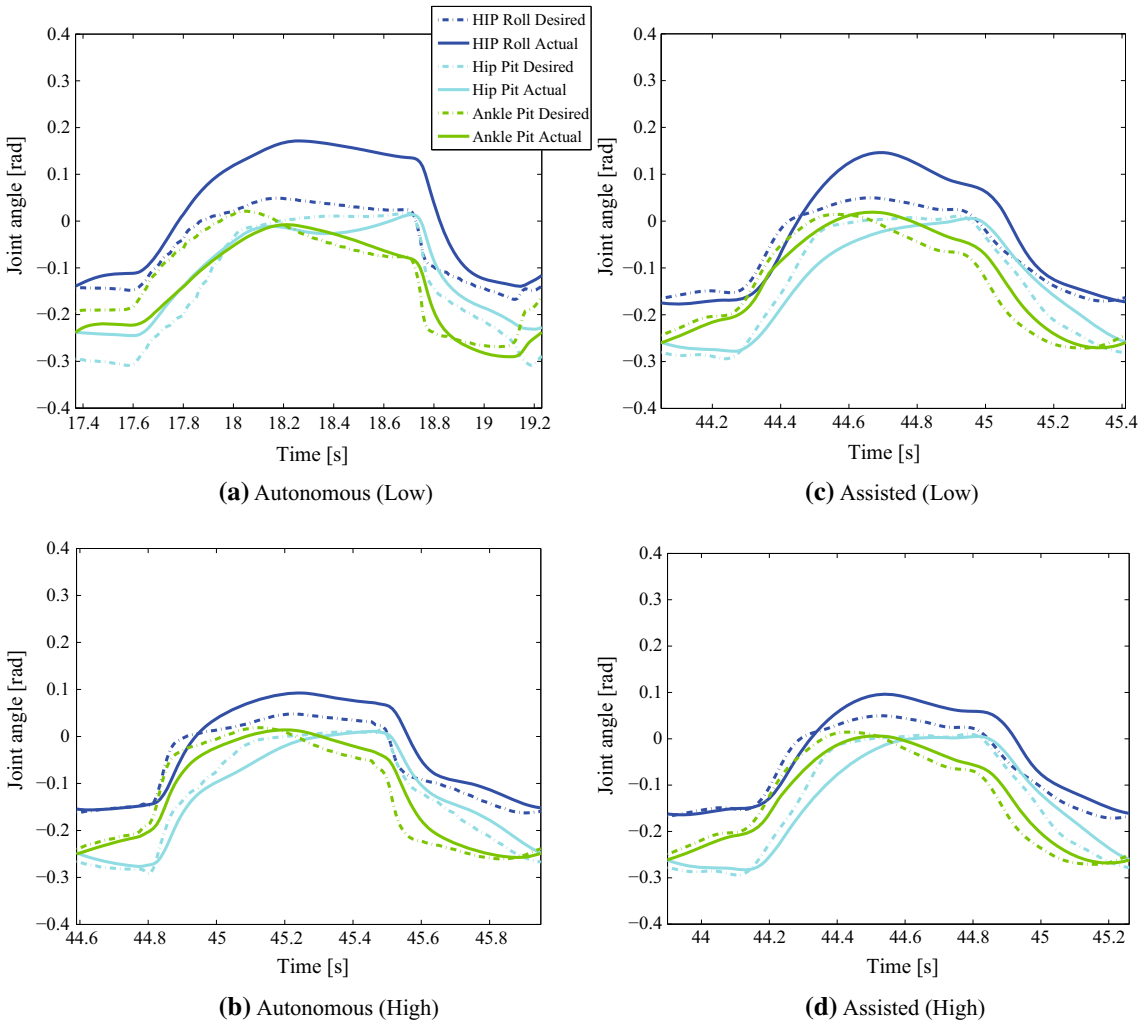

Fig. 16 Representative joint trajectories with references. **a** In autonomous walking with low servo gains, large observed tracking errors between joint angle and reference may be due to torque insufficiency compared with high servo gains in **b**. Our control scheme successfully provides the assistive force to follow the references for both cases with low and high servo gains, as shown in **c** and **d**

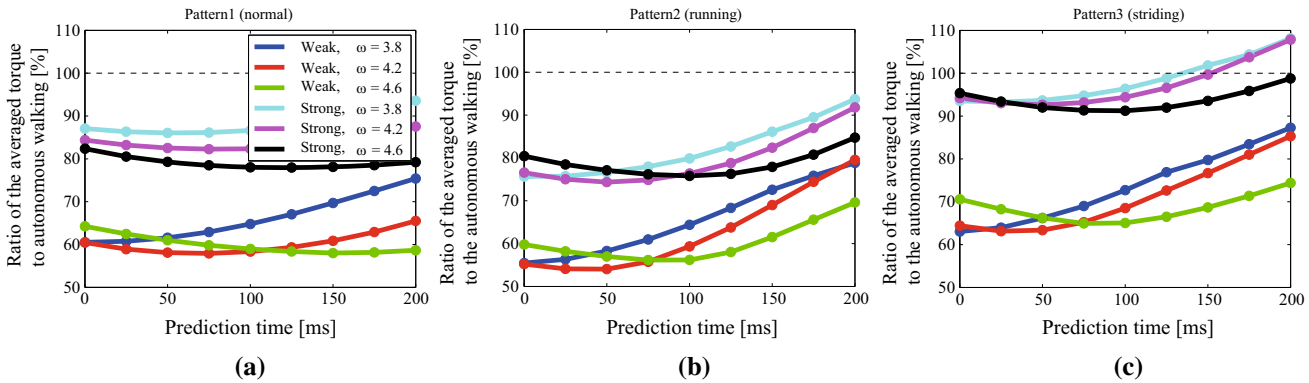

Fig. 17 Ratio of user torques in walking assistance with autonomous walking employed the high servo gains over several prediction times for each walking pattern. **a**–**c** Depict the results for the three different walking patterns as normal, running, and striding, with several walking speeds and servo gains of the user. Overall, our method is more effective for the low-gain user model than the high-gain model. Moreover, prediction becomes more important when walking speed increases

have a data set of walking patterns captured by many subject's walking patterns with natural variations.

Note that simulated physical interaction between the user and the exoskeleton robot models reflects the complex real interaction between the real systems since all the interaction forces at all the connected points are simultaneously calculated even though the physical coupling model itself at each connected point is simple. In our future study, we are planning to apply the proposed framework to a real exoskeleton robot (Hyon et al. 2011).

Acknowledgments This study is the result of Development of BMI Technologies for Clinical Application carried out under SRPBS, MEXT; by MIC-SCOPE; International Cooperative Program, JST and by JSPS and MIZS: Japan-Slovenia research Cooperative Program; by MEXT KAKENHI 23120004; and by JSPS KAKENHI Grant Number 25540085; by ImPACT Program of Council for Science, Technology and Innovation (Cabinet Office, Government of Japan); by the project commissioned by the New Energy and Industrial Technology Development Organization (NEDO).

Appendix 1: Learning procedure of pattern generator model

Data alignment by phase information Focusing on the periodicity of the target motions, we utilize autocorrelative and cross-correlative coefficients for the alignment process. First, we maximize the autocorrelative coefficient for identifying the period T of each sequence as: $T^s \leftarrow \arg\max_j A^s(j)$, where $A^s(j) = \sum_n^N \mathbf{y}_n^{s\,T} \mathbf{y}_{n+j}^s$ is the autocorrelative coefficient with the self-index shift j in phase with a style indexed by s. Next, we maximize the cross-correlative coefficient to find the optimal cross-index shift h in phase as: $h^s \leftarrow \arg\max_j C^s(j)$, where $C^s(j) = \sum_n^N \mathbf{y}_n^{b\,T} \mathbf{y}_{j+\mathrm{rd}\left(\frac{nT^s}{T^b}\right)}^s$ is the cross-correlative coefficient and index b is the style index corresponding to the sequence that has the shortest period. T^b is the period of the shortest period indexed by b. The function $\mathrm{rd}(\cdot)$ is a round-off function. The above procedures yield an aligned data matrix:

$$\mathbf{Y}_a^{\mathrm{all}} = \begin{bmatrix} \mathbf{y}^1_{\mathrm{rd}\left(h^1+\frac{T^1}{T^b}\right)} & \cdots & \mathbf{y}^1_{\mathrm{rd}(h^1+T^1)} \\ \vdots & \ddots & \vdots \\ \mathbf{y}^S_{\mathrm{rd}\left(h^S+\frac{T^S}{T^b}\right)} & \cdots & \mathbf{y}^S_{\mathrm{rd}(h^S+T^S)} \end{bmatrix} \tag{20}$$

where $\mathbf{Y}_a^{\mathrm{all}} = [\mathbf{Y}_a^1 \cdots \mathbf{Y}_a^S]^T \in \mathbb{R}^{DS\times C}$, $\mathbf{Y}_a^s \in \mathbb{R}^{C\times D}$, and C is the number of aligned data samples. Note that each row of the matrix $\mathbf{Y}_a^{\mathrm{all}}$ is the observations corresponding to the same value of the phase ϕ. Each column indicates a corresponding motion sequence indexed by s.

Extraction of observation bases Since the aligned data matrix $\mathbf{Y}_a^{\mathrm{all}}$ is a rectangular matrix, singular value decomposition (SVD)-based matrix factorization can be applied to extract the observation bases. By applying the factorization, we can form a style–content factorial model [referred to as the asymmetric bilinear model in Tenenbaum and Freeman (2000)].

Let $\mathbf{Y}_a^{\mathrm{all}\,\mathrm{VT}}$ be an $S \times DC$ matrix stacked from $DS \times C$ Matrix $\mathbf{Y}_a^{\mathrm{all}}$. Then, SVD for this matrix leads to the following factorial representation as

$$\mathbf{Y}_a^{\mathrm{all}\,\mathrm{VT}} = \mathbf{USV}^T \approx \mathbf{W}\tilde{\mathbf{Y}}. \tag{21}$$

We define the style parameter matrix $\mathbf{W} = [\mathbf{w}^1 \cdots \mathbf{w}^S]^T \in \mathbb{R}^{S\times J}$ to be the first $J(\leq S)$ rows of $\mathbf{U}$, and the content parameter matrix $\tilde{\mathbf{Y}} = ([\bar{\mathbf{Y}}^1 \cdots \bar{\mathbf{Y}}^J]^T)^{\mathrm{VT}} \in \mathbb{R}^{J\times DC}$ to be the first J columns of $\mathbf{SV}^T$. As a result, we can obtain an approximated form as $\mathbf{Y}_a^s \approx \sum_{j=1}^J w_j^s \bar{\mathbf{Y}}^j$. The obtained matrix $\bar{\mathbf{Y}}^j \in \mathbb{R}^{C\times D}$ is named the jth observation basis, and the vector $\mathbf{w}^s \in \mathbb{R}^J$ is the sth style parameter.

Learning a two-factor observation model with bases With the extracted bases $\bar{\mathbf{Y}}^j$ for all j, we can learn the observation model. Since each point of a basis corresponds to a value of phase, we learn a mapping between $\bar{\mathbf{y}}^j$ and $\mathbf{z}$ using all data of each basis. Here we utilize a Gaussian process regression (Rasmussen and Williams 2006) because it allows us to derive an analytically tractable predictive distribution and to learn hyper-parameters by maximization of the marginalized likelihood.

Each basis $\bar{\mathbf{Y}}^j$ is independently modeled as a Gaussian process as $p(\bar{\mathbf{Y}}^j|\mathbf{Z}, \boldsymbol{\beta}^j) \propto \exp\left(-\frac{1}{2}\mathrm{Tr}\left((\mathbf{K}_y^j)^{-1}\bar{\mathbf{Y}}^j(\bar{\mathbf{Y}}^j)^T\right)\right)$ where $\mathbf{Z}$ is the phase-aligned matrix corresponding to $\bar{\mathbf{Y}}^j$ and $\mathbf{z} = \mathbf{h}(\phi) = [\cos(\phi); \sin(\phi)]^T$ is a transformed variable of the phase ϕ to approximately measure the geodesic distance between points on $\mathbb{S}$ as the Euclidean distance in $\mathbb{R}^2$ and $\mathbf{K}_y^j \in \mathbb{R}^{C\times C}$ is the gram matrix in which (p, q) entry is $k_y^j(\mathbf{z}_p, \mathbf{z}_q) = \beta_1^j \exp\left(-\frac{\beta_2^j}{2}||\mathbf{z}_p - \mathbf{z}_q||^2\right) + \delta_{\mathbf{z}_p,\mathbf{z}_q}/\beta_3^j$, and the hyper-parameter is represented as $\boldsymbol{\beta}^j = \{\beta_1^j, \beta_2^j, \beta_3^j\}$. With the above settings, the predictive distribution of the jth basis $\bar{\mathbf{y}}^{j*}$ given a novel input $\mathbf{z}^*$ can be easily derived as $p(\bar{\mathbf{y}}^{j*}|\mathbf{z}^*, \bar{\mathbf{Y}}^j, \mathbf{Z}) = \mathcal{N}(\bar{\mu}^j(\mathbf{z}^*), \bar{\Sigma}^j(\mathbf{z}^*))$ where $\bar{\mu}^j(\mathbf{z}^*) = (\bar{\mathbf{Y}}^j)^T(\mathbf{K}_y^j)^{-1}\mathbf{k}_y^j(\mathbf{z}^*)$, $\bar{\Sigma}^j(\mathbf{z}^*) = \left(k_y^j(\mathbf{z}^*, \mathbf{z}^*) - \mathbf{k}_y^j(\mathbf{z}^*)^T(\mathbf{K}_y^j)^{-1}\mathbf{k}_y^j(\mathbf{z}^*)\right)\mathbf{I}$ and $\mathbf{k}_y^j(\mathbf{z}^*) = [k_y^j(\mathbf{z}^*, \mathbf{z}_1) \cdots k_y^j(\mathbf{z}^*, \mathbf{z}_C)]^T$ (Rasmussen and Williams 2006).

As the result, we extract the mean of the prediction distribution as the basis $\mathbf{f}_j(\cdot) = \bar{\mu}^j(\cdot)$ and obtain the observation model of the adaptive pattern generator in Eq. (2) as

$$\mathbf{y}_c = g(\phi_c, \mathbf{w}_c) = \sum_{j=1}^J w_{c,j}\mathbf{f}_j(\mathbf{h}(\phi_c)). \tag{22}$$

Appendix 2: Two-dimensional coupled oscillator model

Here we consider the behavior of two-dimensional coupled-phase oscillator model of $\{\phi_1, \phi_2\}$ as:

$$\dot{\phi}_1 = \omega_1 + K_1 \sin(\phi_2 - \phi_1), \tag{23}$$
$$\dot{\phi}_2 = \omega_2 + K_2 \sin(\phi_1 - \phi_2) \tag{24}$$

where $\omega_1 > 0$ and $\omega_2 > 0$ are natural frequencies of each oscillator, and K_1 and K_2 are positive coupling gains. The dynamics of the phase difference $\Phi = \phi_1 - \phi_2$ is given as $\dot{\Phi} = \dot{\phi}_1 - \dot{\phi}_2 = (\omega_1 - \omega_2) - (K_1 + K_2)\sin(\Phi)$.

Because of its simple structure, we can easily find two fixed points if $|\omega_1 - \omega_2| < K_1 + K_2$. There is no fixed point if $|\omega_1 - \omega_2| > K_1 + K_2$. A saddle-node bifurcation occurs when $|\omega_1 - \omega_2| = K_1 + K_2$. If $|\omega_1 - \omega_2| < K_1 + K_2$, the coupled oscillator runs with the phase difference $\Phi^* = |\phi_2 - \phi_1| = \sin^{-1}\left((\omega_2 - \omega_1)/(K_1 + K_2)\right)$ and with the compromise frequency $\omega^* = (K_2\omega_1 + K_1\omega_2)/(K_2 + K_1)$ (Strogtz 1994).

Appendix 3: Style–phase estimation procedures

E-step The goal of this step is to compute the estimate for the current state from the estimate for the previous time step and current observation. To this end, we first compute the predictive distribution:

$$\mathbf{x}_{t|t-1} = \mathbf{A}\hat{\mathbf{x}}_{t-1}, \tag{25}$$
$$\Sigma_{x,t|t-1} = \mathbf{A}\hat{\Sigma}_{x,t-1}\mathbf{A}^T + \mathbf{Q}. \tag{26}$$

Then, by using the current observation $\mathbf{y}_t$, the estimate is updated for the current time step:

$$\hat{\mathbf{x}}_t = \mathbf{x}_{t|t-1} + \mathbf{K}_t\left(\mathbf{y}_t - \mu(\mathbf{x}_{t|t-1}; \hat{\mathbf{w}}_{t-1})\right), \tag{27}$$
$$\hat{\Sigma}_{x,t} = \left(\mathbf{I} - \mathbf{K}_t\mathbf{H}_{t|t-1}\right)\Sigma_{x,t|t-1} \tag{28}$$

where

$$\mathbf{H}_{t|t-1} = \left.\frac{\partial \mu(\mathbf{x}; \hat{\mathbf{w}}_{t-1})}{\partial \mathbf{x}}\right|_{\mathbf{x}=\mathbf{x}_{t|t-1}}, \tag{29}$$
$$\mathbf{K}_t = \mathbf{A}\Sigma_{x,t|t-1}\mathbf{H}_{t|t-1}^T\left(\mathbf{H}_{t|t-1}\Sigma_{x,t|t-1}\mathbf{H}_{t|t-1}^T + \mathbf{R}\right)^{-1}. \tag{30}$$

M-step The goal of this step is to update the new style parameter $\hat{\mathbf{w}}$ with the estimate of the state given in E-step and the observation at the current time step. To this end, we define the time-forgetting weighted mean as follows:

$$\ll \cdot \gg_T = \eta_T \sum_{t=1}^{T}\left\{\prod_{s=t+1}^{T}\lambda\right\}(\cdot_t), \tag{31}$$
$$\eta_T = \left\{\sum_{t=1}^{T}\left\{\prod_{s=t+1}^{T}\lambda\right\}\right\}^{-1} \tag{32}$$

where $\lambda (0 \leq \lambda \leq 1)$ is a time-dependent forgetting factor which is introduced for forgetting the effect of the past observations. By using the mean, we can update the style parameter recursively:

$$\hat{\mathbf{w}}_t = \ll \boldsymbol{\mu}^T\boldsymbol{\mu} \gg_t^{-1} \ll \boldsymbol{\mu}^T\mathbf{y} \gg_t \tag{33}$$

where

$$\ll \boldsymbol{\mu}^T\boldsymbol{\mu} \gg_t = (1 - \eta_t) \ll \boldsymbol{\mu}^T\boldsymbol{\mu} \gg_{t-1} + \eta_t \boldsymbol{\mu}(\hat{\mathbf{x}}_t)^T\boldsymbol{\mu}(\hat{\mathbf{x}}_t), \tag{34}$$
$$\ll \boldsymbol{\mu}^T\mathbf{y} \gg_t = (1 - \eta_t) \ll \boldsymbol{\mu}^T\mathbf{y} \gg_{t-1} + \eta_t \boldsymbol{\mu}(\hat{\mathbf{x}}_t)^T\mathbf{y}_t, \tag{35}$$
$$\eta_t = \left\{1 + \frac{\lambda_t}{\eta_{t-1}}\right\}^{-1}, \tag{36}$$
$$\boldsymbol{\mu}(\mathbf{x}_{t|t-1}) = [\mu_y^1(\mathbf{x}_{t|t-1}) \cdots \mu_y^J(\mathbf{x}_{t|t-1})], \tag{37}$$
$$\boldsymbol{\mu}(\hat{\mathbf{x}}_t) = [\mu_y^1(\hat{\mathbf{x}}_t) \cdots \mu_y^J(\hat{\mathbf{x}}_t)]. \tag{38}$$

References

André J, Teixeira C, Santos C, Costa L (2015) Adapting biped locomotion to sloped environments. J Intell Robot Syst 1–16. doi:10.1007/s10846-015-0196-0

Brand M, Hertzmann A (2000) Style machines. In: Proceedings of the 2000 SIGGRAPH, pp 183–192

Degallier S, Righetti L, Gay S, Ijspeert A (2011) Toward simple control for complex, autonomous robotic applications: combining discrete and rhythmic motor primitives. Auton Robot 31(2–3):155–181

Endo G, Morimoto J, Nakanishi J, Cheng G (2004) An empirical exploration of a neural oscillator for biped locomotion control. In: Proceedings of the 2004 IEEE international conference on robotics and automation, pp 3036–3042

Endo G, Morimoto J, Matsubara T, Nakanishi J, Cheng G (2008) Learning CPG-based biped locomotion with a policy gradient method: apply to a humanoid robot. Int J Robot Res 27(2):213–228

Fukuoka Y, Kimura H, Cohen A (2003) Adaptive dynamic walking of a quadruped robot on irregular terrain based on biological concepts. Int J Robot Res 22(3–4):187–202

Gams A, Ijspeert AJ, Schaal S, Lenarcic J (2009) On-line learning and modulation of periodic movements with nonlinear dynamical systems. Auton Robot 27(1):3–23

Hase K, Yamazaki N (1998) Computer simulation of the ontogeny of biped walking. Anthropol Sci 106(4):327–347

Hyon S, Morimoto J, Matsubara T, Noda T, Kawato M (2011) XoR: hybrid drive exoskeleton robot that can balance. In: Proceedings of the IEEE/RSJ international conference on intelligent robots and systems, pp 2715–2722

Kanda T, Ishiguro H, Imai M, Ono T (2003) Body movement analysis of human–robot interaction. In: Proceedings of the international joint conference on artificial intelligence, pp 177–182

Kotosaka S, Schaal S (2000) Synchronized robot drumming by neural oscillator. In: Proceedings of the international symposium on adaptive motion of animals and machines, pp 1–8

Li C, Lowe R, Ziemke T (2014) A novel approach to locomotion learning: actor-critic architecture using central pattern generators and dynamic motor primitives. Front Neurorobot 8(23):1–17

Matos V, Santos CP (2014) Towards goal-directed biped locomotion: combining CPGs and motion primitives. Robot Auton Syst 62(12):1669–1690

Matsubara T, Morimoto J (2013) Bilinear modeling of EMG signals to extract user-independent features for multiuser myoelectric interface. IEEE Trans Biomed Eng 60(8):2205–2213

Matsubara T, Hyon S, Morimoto J (2011) Learning parametric dynamic movement primitives from multiple demonstrations. Neural Netw 24(5):493–500

Matsubara T, Hyon S, Morimoto J (2012) Real-time stylistic predictions for whole-hody human motions. Neural Netw 25(1):191–199

Matsubara T, Morimoto J, Nakanishi J, Sato M, Doya K (2006) Learning CPG-based biped locomotion with a policy gradient method. Robot Auton Syst 54:911–920

Matsuoka K (1985) Sustained oscillations generated by mutually inhibiting neurons with adaptation. Biol Cybern 52:367–376

Michalowski MP, Kozima H, Abanovi S (2007) A dancing robot for rhythmic social interaction. In: Proceedings of the ACM/IEEE international conference on human–robot interaction, pp 1–8

Morimoto J, Noda T, Hyon S (2012) Extraction of latent kinematic relationships between human users and assistive robots. In: Robotics and automation (ICRA), 2012 IEEE international conference on, pp 3909–3915

Morimoto J, Endo G, Nakanishi J, Cheng G (2008) A biologically inspired biped locomotion strategy for humanoid robots: modulation of sinusoidal patterns by a coupled oscillator model. IEEE Trans Robot 24(1):185–191

Nakamura Y, Mori T, Sato M, Ishii S (2007) Reinforcement learning for a biped robot based on a CPG-actor-critic method. Neural Netw 20(6):723–735

Nakanishi J, Morimoto J, Endo G, Cheng G, Schaal S, Kawato M (2004) Learning from demonstration and adaptation of biped locomotion. Robot Auton Syst 47(2–3):79–91

Nassour J, Hénaff P, Benouezdou F, Cheng G (2014) Multi-layered multi-pattern CPG for adaptive locomotion of humanoid robots. Biol Cybern 108(3):291–303

Rasmussen CE, Williams CKI (2006) Gaussian processes for machine learning. MIT Press, Cambridge

Righetti L, Ijspeert AJ (2006) Programmable central pattern generators: an application to biped locomotion control. In: Proceedings of the IEEE international conference on robotics and automation, pp 1585–1600

Righetti L, Buchli J, Ijspeert AJ (2006) Dynamic hebbian learning in adaptive frequency oscillators. Phys D 216(2):269–281

Ronsse R, Vitiello N, Lenzi T, van den Kieboom J, Carrozza M, Ijspeert A (2010) Adaptive oscillators with human-in-the-loop: proof of concept for assistance and rehabilitation. In: Proceedings of the IEEE international conference on biomedical robotics and biomechatronics, pp 668–674

Ronsse R, Lenzi T, Vitiello N, Koopman B, vanAsseldonk E, Rossi SD, van den Kieboom J, van der Kooij K, Carrozza M, Ijspeert A (2011) Oscillator-based walking assistance: a model-free approach. In: Proceedings of the IEEE international conference on rehabilitation robotics 2011, pp 1–6

Silva P, Santos CP, Matos V, Costa L (2014) Automatic generation of biped locomotion controllers using genetic programming. Robot Auton Syst 62(10):1531–1548

Strogtz SH (1994) Nonlinear dynamics and chaos. Westview Press, Cambridge

Suzuki K, Mito G, Kawamoto H, Hasegawa Y, Sankai Y (2007) Intention-based walking support for paraplegia patient with robot SuitHAL. Adv Robot 21(12):1441–1469

Taga G, Yamaguchi Y, Shimizu H (1991) Self-organized control of bipedal locomotion by neural oscillators in unpredictable environment. Biol Cybern 65:147–159

Taylor GW, Hinton GE (2009) Factored conditional restricted Bolzmann machines for modeling motion style. In: Proceedings of the 26th annual international conference on machine learning, 2009, pp 1025–1032

Tenenbaum JB, Freeman WT (2000) Separating style and content with bilinear models. Neural Comput 12(6):1247–1283

Tsuchiya K, Aoi S, Tsujita K (2003) Locomotion control of a biped locomotion robot using nonlinear oscillator. In: Proceedings of the 2003 IEEE/RSJ international conference on intelligent robots and systems, pp 1745–1750

Wang JM, Fleet DJ, Hertzmann A (2007) Multifactor Gaussian process models for style-content separation. In: Proceedings of the 24th annual international conference on machine learning, pp 975–982

Zhang X, Hashimoto M (2009) SBC for Motion Assist Using Neural Oscillator. In: Proceedings of the IEEE international conference on robotics and automation 2009, pp 659–664